

X-ray and multi-wavelength analysis of candidate AGNs in dwarf galaxies in the Boötes field

RUJUTA A. PUROHIT ,¹ RYAN C. HICKOX ,¹ AND GRAYSON C. PETTER ,¹

¹*Department of Physics and Astronomy, Dartmouth College, 6127 Wilder Laboratory, Hanover, NH 03755, USA*

ABSTRACT

We present a multi-wavelength analysis of three candidate Active Galactic Nuclei (AGNs) in dwarf galaxies in the Boötes field. Dwarf galaxies are particularly interesting hosts for AGNs as they may contain central black holes that have not grown significantly since the epoch of their formation in the early universe. Using data from the Chandra X-ray Observatory, we find three X-ray luminous dwarf galaxies and we assess their candidacy as AGNs with standard emission-line diagnostics. We compute the X-ray, mid-infrared, and [O III] luminosities and compare them to established relationships in the literature. We then fit various star-forming and AGN templates to the spectral energy distributions (SEDs). The star formation rates estimated from the SED fits are unable to explain the observed X-ray luminosities of two of the candidates, providing more support for the presence of AGNs. We then use various scaling relations, in particular the relationship between BH mass and stellar velocity dispersion, to estimate the masses of the BHs to be $\sim 10^5 - 10^6 M_\odot$, in the intermediate-mass black hole (IMBH) regime. Finally, we find these systems to be obscured (with $\log N_{\mathrm{H}} [\mathrm{cm}^{-2}] < 24.2, 24.8$, and 23.8, respectively) and accreting at Eddington ratios $10^{-2} < \lambda_{\mathrm{Edd}} < 10^{-1}$. Studying dwarf galaxies, AGNs, and IMBHs can help us understand the formation and evolution of galaxies-BHs in the early universe and can also shed light on probable BH seeds. Wide-field X-ray surveys could reveal more of these obscured, rapidly accreting sources and are thus a promising way to search for IMBHs in the local universe.

1. INTRODUCTION

It is widely accepted that a supermassive black hole (SMBH, $M_{\mathrm{BH}} \approx 10^6 - 10^{10} M_\odot$) lies at the center of nearly all local massive galaxies (e.g., Magorrian et al. 1998; Marconi & Hunt 2003; Kormendy & Ho 2013). The majority of SMBHs lie dormant but a small fraction produce significant amounts of light and energy, often outshining the whole host galaxy across the electromagnetic spectrum, resulting in an active galactic nucleus (AGN; e.g., Hickox & Alexander 2018; Masini et al. 2020). The accretion of gas onto the SMBH produces an optically thick disk of material called the accretion disk. An AGN is the observed physical manifestation of this gas accretion (for reviews see e.g., Salpeter 1964; Lynden-Bell 1969; Shakura & Sunyaev 1973; Rees 1984; Padovani et al. 2017; Hickox & Alexander 2018).

There are many theories for the formation of SMBHs (e.g., Miller et al. 2015; Greene et al. 2020): the collapse of primordial gas (“heavy” seeds of $\sim 10^5 M_\odot$; e.g., Loeb

& Rasio 1994; Begelman et al. 2006; Johnson et al. 2013; Ferrara et al. 2014), super-Eddington accretion of Population III star BH remnants in the early-universe (“light” seeds of $\sim 10^2 M_\odot$; e.g., Madau & Rees 2001; Whalen & Fryer 2012; Taylor & Kobayashi 2014; Jiang et al. 2019), and models that involve a gradual gravitational runaway effect (e.g., Portegies Zwart & McMillan 2002; Miller & Hamilton 2002). The challenge to testing these theories is that they require extensive multi-wavelength observations of high-redshift galaxies. Such detailed observations of early-universe systems were not possible until the recent advent of the James Webb Space Telescope (e.g., Volonteri & Reines 2016; Vito et al. 2018; Larson et al. 2023). These early-universe observations of red nuggets (e.g., Barro et al. 2023; Greene et al. 2023) and broad-line AGNs (Kokorev et al. 2023) are helping place constraints on the models of BH-galaxy co-evolution.

Aside from high-redshift observations, studying BHs in the local-universe is a complementary method to study BH seeds and evolution. Local systems would allow us to place constraints on the BH masses when they first formed and give us clues about how they may have evolved.

Corresponding author: Rujuta A. Purohit
rujuta.purohit.24@dartmouth.edu

Currently, only one BH formation channel is well-established: a BH is the remnant of a collapsed stellar core following a supernova at the end of a massive ($> 8M_{\odot}$) star's evolution. These BHs have masses of the order $\sim 3 - 10 M_{\odot}$ (e.g., Celotti et al. 1999; Remillard & McClintock 2006; Bambi 2020), and the upper limit is $50 M_{\odot}$, imposed by pulsational pair instability (Heger et al. 2003; Woosley 2017). If BHs are formed only from the deaths of stars, there must be some mechanism by which these BHs grow to be the SMBHs we observe today. It is believed that BHs in a mass range between stellar BHs and SMBHs had to exist. This is supported by the fact that SMBHs are not observed until at least $z = 8.7$ (e.g., Larson et al. 2023). Thus, these BHs in the mass gap between stellar mass and SMBHs are called intermediate-mass black holes (IMBHs) (e.g. Greene et al. 2020; Volonteri et al. 2021). IMBHs as seeds are excellent systems to study as their mass and Eddington ratios may reveal the history of BH growth.

IMBHs (see Greene et al. (2020) for a review) are defined to have masses in the range $100 - 10^5 M_{\odot}$. Finding IMBHs and characterizing their nature is of interest for many reasons, such as finding clues about the origins of SMBHs and probing BH feedback mechanisms in lower mass systems. One of the biggest hurdles has been detecting them (e.g., Nguyen et al. 2018; Baldassare et al. 2020). Through analyses of SMBHs and their host galaxies, many scaling relations have been defined that relate to their physical properties. One such scaling relation is between the BH mass and the host galaxy's total stellar mass (e.g., Mancini & Feoli 2012; Reines & Volonteri 2015). Thus, since we know that central SMBH mass correlates with the galaxy mass, we might expect the same for IMBHs in the smallest galaxies. This allows us to essentially verify whether dwarf galaxies ($M_{\star} < 10^9 M_{\odot}$) host IMBHs. While there are no dynamically confirmed IMBHs in or without dwarf galaxies, recent studies have produced a number of promising candidates (e.g., Jardel & Gebhardt 2012; Neumayer & Walcher 2012; Nguyen et al. 2018).

The IMBHs and AGNs found in dwarf galaxies would be crucial for constraining BH seed formation models and better understanding the distribution of BH mass throughout the universe (e.g., Wasleske et al. 2022). Dwarf galaxies at low redshift may host BHs of similar mass to those in early-universe galaxies and so provide a probe of their early formation (e.g., Greene et al. 2020; Latimer et al. 2021). In the local universe, it is estimated that $\sim 80\%$ of nearby, low-mass early-type galaxies host BHs (Nguyen et al. 2018), but the total population of BHs in low-mass galaxies remains poorly constrained. This is significant, considering the first two

prototype low-mass AGNs hosting IMBHs were detected in the local universe ($z < 0.025$) (NGC 4395 Filippenko & Sargent 1989; Filippenko & Ho 2003) and (POX 52 Kunth et al. 1987; Barth et al. 2004). Thus, searching for AGNs in dwarf galaxies is a valuable method for identifying IMBHs (e.g., Reines et al. 2013; Greene et al. 2020).

Generally, the X-ray energy bands are considered to be the most reliable in detecting accreting SMBHs (and hopefully IMBHs), due to their high contrast with the host galaxy and strong penetrating power (e.g. Brandt & Alexander 2015). However, even X-ray-selected samples suffer some bias against obscured sources (e.g., Hickox & Alexander 2018; Masini et al. 2020). Thus, in this paper, we use X-ray emission to guide our primary search for targets, but then follow up with multi-wavelength data by studying relationships between luminosities at different wavelengths and host galaxy properties (such as the stellar mass, M_{\star} , star formation rate (SFR), and stellar bulge velocity dispersion, σ^*).

This paper is organized as follows: §2 details our search process, data, and the sample of targets studied. We calculate the X-ray luminosity from flux values in the Chandra catalog and use these to guide our selection process. In §3, we compare the observed properties of our targets in reference to established relationships in literature. We carry out a SED template fitting and analyze the mid-infrared (MIR) and [O III] luminosities. In §4, we estimate the masses of the BHs in the candidate AGNs through different scaling relations. We also calculate the corresponding Eddington limits and ratios to better interpret our findings. §5 summarizes our results and details the scope for future work.

In this work, we adopt a “Planck 2015” Λ -CDM cosmology (Planck Collaboration et al. 2016): $H_0 = 67.8 \text{ km s}^{-1} \text{ Mpc}^{-1}$, $\Omega_m = 0.308$, and $\Omega_{\Lambda} = 0.692$.

2. DATA

Our approach to identifying IMBH candidates is to search for X-ray counterparts to dwarf galaxies, as luminous X-ray emission is an unambiguous indicator of AGN activity in a galaxy (e.g., Miller et al. 2015; Pardo et al. 2016; Baldassare et al. 2015). This search requires deep and overlapping optical and X-ray data as dwarf galaxies are expected to have intrinsically low luminosity. The X-ray waveband identifies AGNs while the optical provides initial estimates of redshift and stellar mass. Given the low number of IMBH candidates in the literature (for a list of recent candidates, see Greene et al. 2020), a wide-field search would provide a large number of objects to study. The analysis would also benefit from panchromatic photometry to study the host galaxy

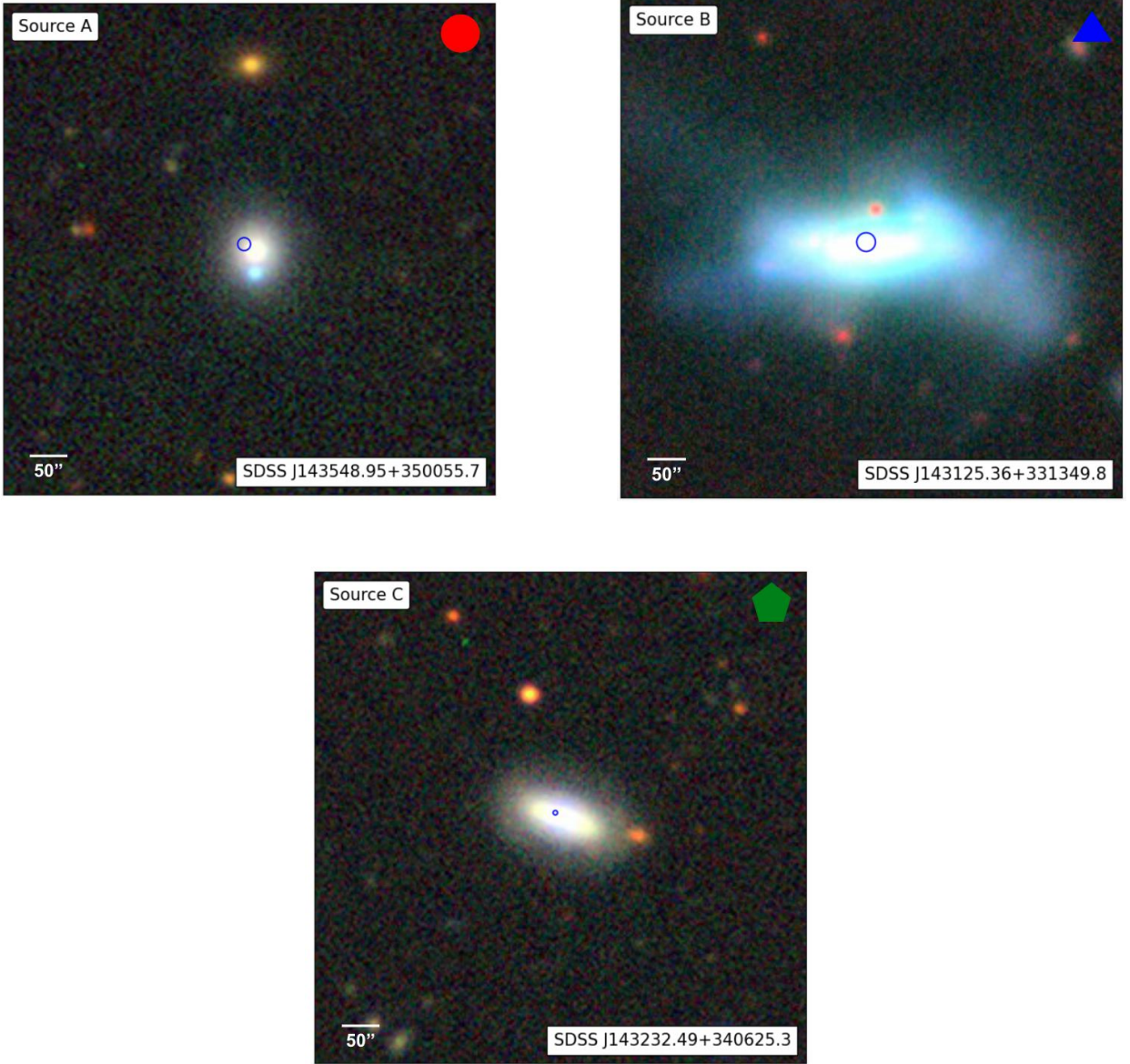


Figure 1. Optical-NIR (g , r , z) color images of our sample of local ($z < 0.1$) dwarf galaxies ($M_* < 10^9 M_\odot$) in the Boötes field with candidate X-ray AGN potentially powered by IMBHs. The images are obtained from the DESI Legacy Sky Survey Browser. The object name of each source is listed in the top left corner and the chosen icon used throughout this work is shown in the top right corner. The blue circles are centered on the coordinates of the X-ray source detected by Chandra and the radii of the circles are equal to the positional error. The scale is shown in the lower left corner. *Image credit:* Legacy Surveys / D. Lang (Perimeter Institute)

and AGN properties through spectral energy distribution modeling. The 9 square degree Boötes extragalactic survey field satisfies all of these requirements because of the investment of deep X-ray to far-infrared photometry, spectroscopy, and analysis. We utilize two catalogs in this work, the Chandra Deep Wide-Field Survey in the Boötes Field (Masini et al. 2020) for X-ray source identification, and the photometric redshift and stellar

mass catalog that includes the Boötes field from Duncan et al. (2021). Optical and IR obtained from photometry on NASA/IPAC Extragalactic Database (NED)¹ allows us to calculate initial estimates of the sources' luminosities, distances, and star formation rates.

¹ <https://ned.ipac.caltech.edu/>

Table 1. Physical properties of the targets studied in this work

| Object Name | Identifier | Redshift | Chandra exposure time | $\log L_X$ | $\log L_{\text{MIR}}$ | $\log L_{[\text{OIII}]}$ |
|--------------------------|------------|----------|-----------------------|----------------------|-----------------------|--------------------------|
| | | | (s) | (erg s $^{-1}$) | (erg s $^{-1}$) | (erg s $^{-1}$) |
| SDSS J143548.95+350055.7 | A | 0.0285 | 28199.4 | $40.1^{+0.3}_{-0.2}$ | 40.1 | 39.1 |
| SDSS J143125.36+331349.8 | B | 0.0226 | 22072.8 | $40.3^{+0.2}_{-0.1}$ | 42.1 | 40.7 |
| SDSS J143232.49+340625.3 | C | 0.0423 | 45452.4 | $41.1^{+0.1}_{-0.1}$ | 43.6 | 40.7 |

NOTE—The main properties of the three targets we study in this paper. *Column 1:* Object Name. *Column 2:* Assigned identified used to refer to the source in this work. The identifier along with the chosen symbol are shown in Figure 1. *Column 3:* Spectroscopic redshift as reported in Duncan et al. (2021). The spectroscopic values supersede the photometric ones when available. *Column 4:* Exposure time of Chandra. *Column 5:* X-ray luminosity using flux from Masini et al. (2020) and redshift-converted-distance. *Column 6:* MIR luminosity calculated in §3.1. *Column 7:* [O III] luminosity using SDSS line fluxes. The errors in luminosity are fractional.

We matched the catalog of the X-ray sources (Masini et al. 2020) with the optical-IR positions of galaxies in (Duncan et al. 2021) with a matching radius of 1''. The Duncan et al. (2021) catalog contains the stellar mass estimates we use to identify dwarf galaxies. This initial cross-match revealed 168 total sources. Since we require optical-IR data for our planned analysis, we maintained those sources in our sample that had multi-wavelength photometry on NED. For objects in the local universe, we limited the sample to $z < 0.05$, making redshift cuts using the values reported in Duncan et al. (2021) which are a combination of photometric and spectroscopic values. For the Boötes field, the spectroscopic-zs are taken primarily from SDSS. The photometric values are obtained through SED fits and are superseded by the spectroscopic ones whenever applicable.

We selected local dwarf galaxy candidates by making cuts on stellar mass as $M_\star < 10^{9.5} M_\odot$ to define our dwarf galaxy sample. The stellar masses in Duncan et al. (2021) are derived using a simpler grid-based SED fitting approach that scales to the large samples available across the Boötes field. We realized that for nearby galaxies, M_\star might be underestimated in Duncan et al. (2021) because the method uses 3'' apertures for optical to NIR bands and 4'' apertures for the IR. This aperture measures a much smaller fraction of light from large sources like nearby galaxies (see Duncan et al. (2021) Section 2.1 for more details). Thus, due to the choice of the aperture sizes, M_\star estimated through aperture photometry will be systematically underestimated for local objects with large angular diameters. Previous cuts made for optical spectra allowed us to examine our dwarf galaxy sample using velocity dispersion estimates. Any objects with $\sigma^* > 150 \text{ km s}^{-1}$ were bound to have

a larger mass than reported if they were present in our low-mass subset. We found 14 sources with $\sigma^* > 150 \text{ km s}^{-1}$.

We further discarded 5 sources that either had very low X-ray fluxes ($F_X \geq 10^{-16} \text{ erg s}^{-1} \text{ cm}^{-2}$) or no listed values. After this elimination, we were left with three sources that we analyze in this paper.

We calculated the X-ray luminosities of the sources using flux values listed in the *Chandra Deep Wide-Field Survey in the Boötes Field* catalog (Masini et al. 2020). The luminosities of the three targets, along with their coordinates and Duncan et al. (2021) reported masses are listed in Table 1.

We obtained optical-NIR multiband images of the sources from the DESI Legacy Sky Survey Browser². The images are shown in Figure 1. The identification is displayed as a circle centered at the coordinates of the X-ray source with a radius equal to the positional uncertainty. The images are from the Legacy Surveys Data Release 9 and contain the three optical-NIR bands g , r , z .

The optical narrow-line emission observed in SDSS spectra also provide a useful check for identifying these sources as AGNs. Figure 2 shows all three targets on a narrow-line [N II]/H α vs. [O III]/H β Baldwin, Phillips & Terlevich (BPT) diagnostic diagram (Baldwin et al. 1981) with demarcations determined by Kewley et al. (2006). We plot these using the line measurements that come from spectra reported in SDSS DR17 using the Science Archive Server (SAS³; Abdurro'uf et al. 2022). Sources A and C lie in the AGN region while B lies in the star-forming region (although with significant un-

² <https://www.legacysurvey.org>

³ <https://dr17.sdss.org/home>

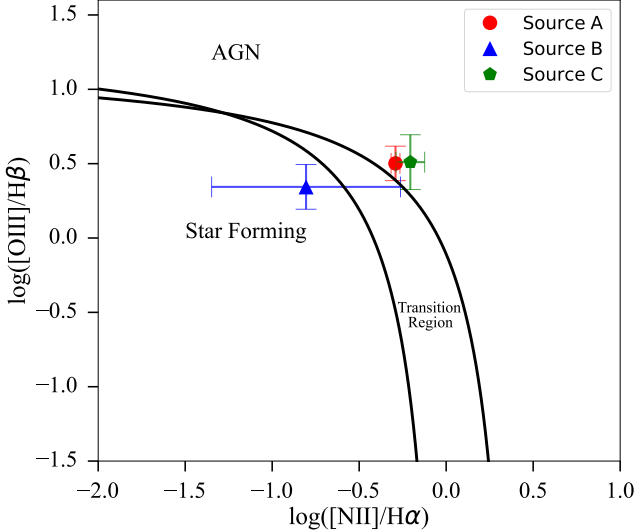


Figure 2. The 3 dwarf galaxies we study in this work are placed on a narrow-line BPT diagnostic diagram (Baldwin et al. 1981) with demarcations as determined by Kewley et al. (2006). Two of the targets (A and C) clearly lie in the AGN-demarcated region while the uncertainty on source B’s line ratios do not permit a robust characterization of the ionization source. This analysis serves as the first test for these targets’ AGN candidacy. Because the ionization source of B is not well constrained, we continue to study it as a potential AGN in this work.

certainty in [NII]/Halpha). We include Source B in our sample due to error bars on the x -axis of the BPT diagram ($\log [NII]/H\alpha$) extending to the AGN region.

3. ANALYSIS

3.1. Spectral Energy Distribution (SED)

To further investigate whether our three candidate dwarf AGN contain growing black holes, we begin by creating SEDs for each source. SED fitting can decompose the emission of a galaxy into its component parts, and allow us to measure galaxy properties such as M_* , SFR, AGN luminosity, etc. (e.g., Magris C. et al. 2015; Yamada et al. 2023).

We utilize SED fitting in the wavelength range $0.15 \mu\text{m} < \lambda < 25 \mu\text{m}$ obtained from NED. The data used come from GALEX (Martin et al. 2005) for the UV, SDSS DR17 (Abdurro’uf et al. 2022) for the optical-NIR, the Wide-field Infrared Survey Explorer (Wright et al. 2010, WISE), and the Spitzer Space Telescope (Werner et al. 2004) for the MIR. In the far-IR, we use data from the Herschel Space Telescope’s Photodetector Array Camera and Spectrometer (PACS) and Spectral and Photometric Imaging Receiver (SPIRE), as compiled by the HELP catalog (Shirley et al. 2021). For overlapping wavebands, we use the flux values with the

higher signal-to-noise and/or the more recent observation.

We use the Code Investigating GALaxy Emission (CIGALE; Burgarella et al. 2005; Boquien et al. 2019) to fit the SED to different galaxy types which gives us important initial insights into the spectral properties of these galaxies and allows us to estimate the AGN luminosity. Within CIGALE we utilize the AGN emission model `dale2014` (Dale et al. 2014), the dust attenuation model `dustatt_calzleit` (Calzetti et al. 2000), and various star formation history models.

To check our results from CIGALE, we also carry out SED fitting using the templates from the low-resolution templates from Assef et al. (2010). The templates in Assef et al. (2010) are generated using empirical data from the multi-wavelength photometric observations of the NDWFS (Jannuzi et al. 1999) and the spectroscopic observations of AGES (Kochanek et al. 2012) which cover the Boötes field extensively. Using the SEDs, we estimate the AGN contribution to the MIR luminosity, L_{MIR} , by interpolating the luminosity of the AGN component to its monochromatic value of νL_ν $6\mu\text{m}$.

3.2. X-ray and Mid-IR Luminosity Relation

There is an empirical relationship between the X-ray and MIR luminosities of AGN (e.g., Gandhi et al. 2009; Stern 2015) which we explore in this section. We obtain the MIR luminosity from the SED fitting, as described in Section 3.1. We use the integrated scaling relation from Chen et al. (2017) to compare the X-ray and mid-IR emission from the AGN. Along with our targets, we also plot local AGN as listed in Gandhi et al. (2009) to compare our sample of targets to previous studies. This is shown in Figure 4.

We use the monochromatic $6\mu\text{m}$ MIR luminosity since this is used by Chen et al. (2017) to study the $L_{\text{X}} - L_{\text{MIR}}$ relation. The intrinsic dispersion in the relationship is 0.23 dex (Carroll et al. 2023). We see that our targets are found at the lower end of the trend. Their MIR luminosities are consistent with those of other AGNs but the significant deviation (≥ 1 dex) from the lowest X-ray luminosities suggests significant obscuration.

The deviation from the linear relationship can be used to study the AGNs’ obscuration (e.g., Carroll et al. 2021). We first check the hardness ratios ($\text{HR} = (\text{H} - \text{S})/(\text{H} + \text{S})$ where H are hard X-ray counts and S are soft X-ray counts) computed from Chandra’s observed flux values in Masini et al. (2020) that used the Bayesian Estimator for Hardness Ratio (BEHR, Park et al. 2006). The hardness ratios for sources A, B, C are $\text{HR} = -0.54^{+0.15}_{-0.46}$, $-0.14^{+0.32}_{-0.25}$, $-0.59^{+0.078}_{-0.09}$ respectively. Even though the hardness ratios seem low, we estimate

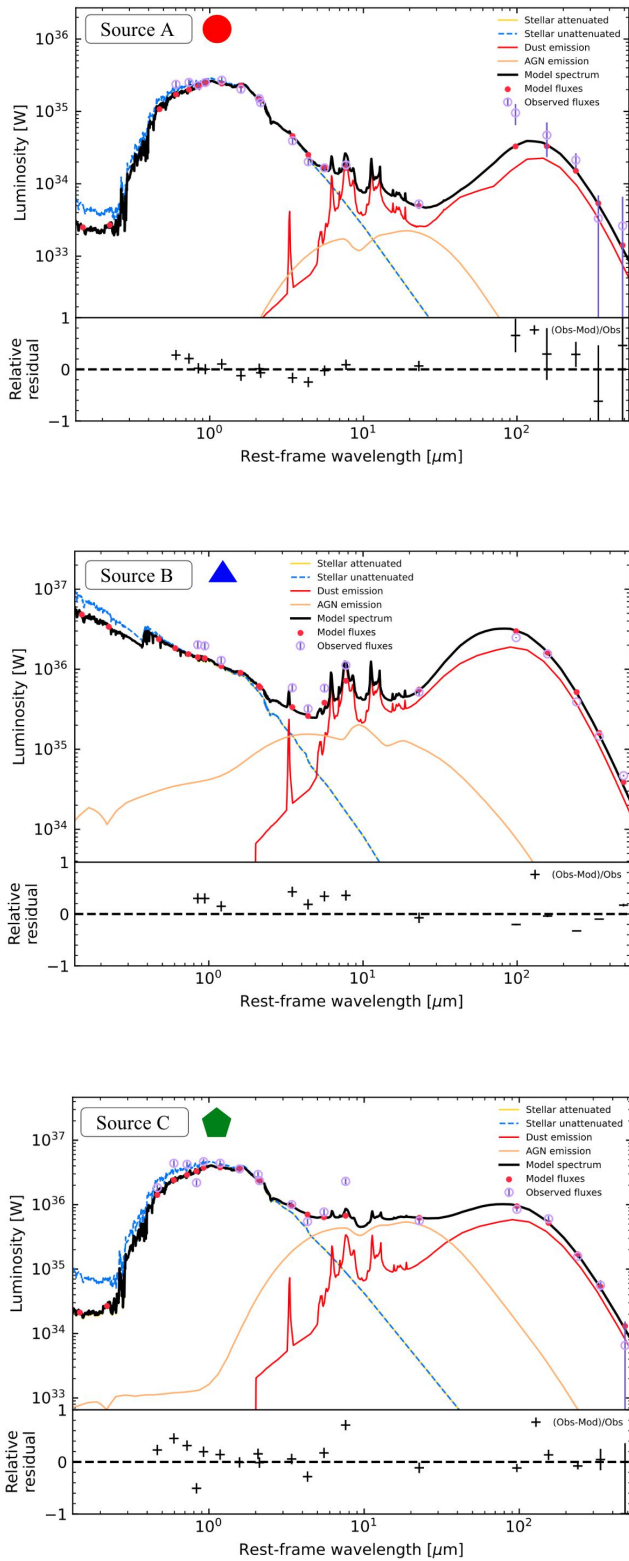


Figure 3. The results of SED fitting using photometric data done in CIGALE. The models used in the fitting describe the star formation history, AGN structure, and dust attenuation. The errors in the flux values are taken into account when we perform the fitting and are also plotted.

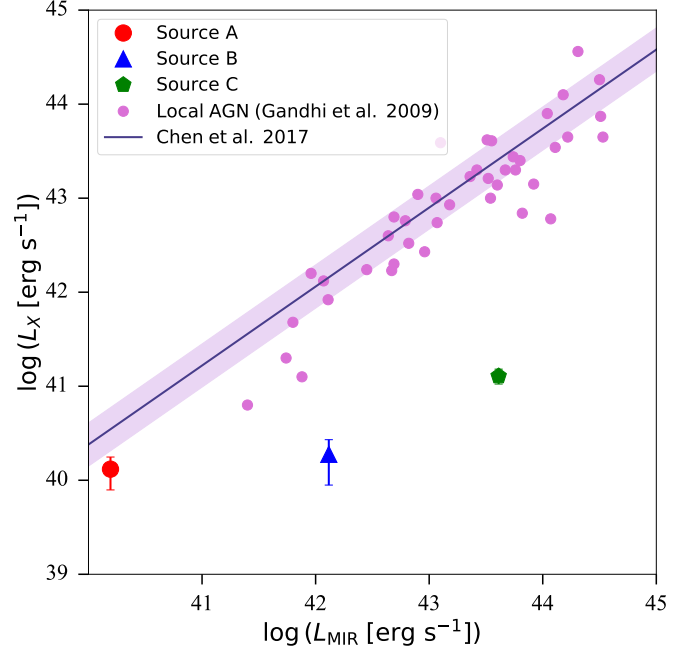


Figure 4. A plot of the derived MIR vs the X-ray luminosities of the 3 galaxies along with the integrated scaling relation in Chen et al. (2017). The MIR luminosities are derived by integrating over the AGN components of the SED fitting. We also plot a sample of local AGN from Gandhi et al. (2009) (solid pink circles) for reference. Our sources fall in the low-luminosity tail of the scatter. The deviation from the linear relationships suggests significant obscuration that we estimate using Carroll et al. (2021).

the column densities (N_{H}) following Carroll et al. (2021) which uses a BORUS model that relates N_{H} to the ratio of the observed to expected L_{X} . We use the scatter in the relationship to get upper limits on the values of N_{H} . For sources A, B, and C, $\log N_{\text{H}} < 23.7, 24.8, 23.8$.

3.3. $[\text{O III}]$ Emission Line Relations

The scaling relationships between L_{X} and $L_{[\text{OIII}]}$ have been widely studied (e.g., Georgantopoulos & Akylas 2010; Bongiorno et al. 2010; Yan et al. 2011). The relationships between $L_{[\text{OIII}]}$ and L_{MIR} are also well defined (e.g., LaMassa et al. 2010; Georgantopoulos & Akylas 2010). The $[\text{O III}]$ luminosity is considered to be a good proxy of nuclear power because it originates from the narrow-line region which is outside the obscuring dusty torus and is usually regarded as an isotropic luminosity indicator (e.g., Bassani et al. 1999; Georgantopoulos & Akylas 2010; Yan et al. 2011). Emission lines are studied to probe the nuclear activity in AGNs and they provide constraints on the physical models and theories of AGN and galaxy co-evolution (e.g., Nandra 2006; Bongiorno et al. 2010; Feltre et al. 2016; Marziani et al. 2017).

Together, the [O III] and intrinsic X-ray luminosities are good indicators for the AGN bolometric luminosity (Heckman et al. 2004). Among Type 1 AGNs, for which there is an unobstructed view of the accretion disk, L_X is found to correlate very well with $L_{[\text{OIII}]}$ (e.g., Mulchaey et al. 1994; Heckman et al. 2005). Comparing L_X with $L_{[\text{OIII}]}$ can thus also reveal the level of X-ray absorption.

We obtain the [O III] line fluxes from SDSS DR 17. The extracted flux is corrected for obscuration using the following equation from Bassani et al. (1999):

$$F_{\text{corr}} = F_{\text{obs}} \left[\left(\frac{H\alpha}{H\beta} \right) / \left(\frac{H\alpha}{H\beta} \right)_0 \right]^{2.94} \quad (1)$$

where $\left(\frac{H\alpha}{H\beta} \right)_0$ is the intrinsic Balmer decrement equal to 2.85 (Yan et al. 2011).

We determine the contribution of the AGN to the galaxy's composite [O III] luminosity using the tracks plotted in Jones et al. (2016). The AGN contribution is based on the relative distance in the BPT diagram of the source from pure star-forming and pure AGN regions. We derive and compare these from the BPT diagram in Figure 2. Sources A, B, C have an AGN contribution to the [O III] luminosity of 90%, 50% (treated as an upper limit given the errors in the emission lines of source B as seen in Figure 2), and 80% respectively. With the corrected, AGN-only luminosity, we present the plot of $L_{[\text{OIII}]}$ vs L_X in Figure 5.

There is also a well-studied relationship between emission line luminosities and the MIR luminosities (e.g. LaMassa et al. 2010; Yan et al. 2011). We examine the relationship between the [O III] and the MIR as described in LaMassa et al. (2010). We plot the values of the targets, along with the data sets used in LaMassa et al. (2010) in Figure 6. We see that the targets fall within the scatter of the relationship as the trend continues to low luminosities.

We also calculate N_H using the $L_X - L_{[\text{OIII}]}$ relationship for Type 2 Seyferts by calculating the expected L_X . This allows us to make rough estimates on N_H . For sources A, B, C, we obtain limits of $\log N_H < 24.2, \sim 24.2$, and 23.2, respectively.

3.4. Emission from X-ray binaries

To confirm that the X-ray emission that we observe produced by AGN activity, we calculate the luminosity that we would observe from X-ray binaries within these galaxies. Chandra studies of nearby star-forming late-type galaxies and passive early-type galaxies have shown that the X-ray point-source emission from relatively young high-mass X-ray binaries and older low-mass X-ray binaries correlates well with galaxy SFR and

M_\star , respectively (eg., Grimm et al. 2003; Gilfanov 2004; Lehmer et al. 2010).

Lehmer et al. (2010) describes a linear relationship between galaxy-wide emission from X-ray binaries (L_{XB}), SFR, and M_\star as:

$$L_X^{\text{gal}} = \alpha M_\star + \beta \text{SFR} \quad (2)$$

where $\alpha = 9.05 \pm 0.37 \times 10^{28}$ (erg M_\odot^{-1} s $^{-1}$) and $\beta = 1.62 \pm 0.22 \times 10^{39}$ (erg M_\odot s $^{-1}$ yr $^{-1}$).

We obtain the SFR from the SED fitting described in §3.1. This value is listed in Table 2. To obtain another estimate, we use the equation from Calzetti (2013) which derives the SFR using the H α luminosity. We calculate the H α luminosity, $L_{\text{H}\alpha}$, by using the flux values reported in the SDSS DR17 accessed through SAS (Blanton et al. 2017) and are listed in Table 2.

$$\text{SFR} = 5.5 \times 10^{-42} L_{\text{H}\alpha} \quad (3)$$

The approach we adopt uses a conservative method for estimating $L_{\text{H}\alpha}$. Instead of removing the AGN contribution from the integrated $L_{\text{H}\alpha}$ galaxy emission, we assume that all the emission is from stellar processes. This method gives us the upper limits on the quantities we calculate which are enough to compare the estimated L_{XB} against the observed L_X . Furthermore, we find that using the SED-derived SFR gives us higher values than using the $L_{\text{H}\alpha}$ -derived ones and thus we report these to be more conservative. We also check the SFRs reported in the Herschel Extragalactic Legacy Project (HELP; Shirley et al. 2021) that are evaluated using radio emission analysis. With Equation 2, we find that using radio SFRs does not significantly affect the values of L_{XB} . The radio-SFR are consistent with the errors we get from the $L_{\text{H}\alpha}$ and SED. The difference in the optical and radio SFRs can be attributed to extinction in different wavelength regimes among other reasons.

The stellar masses listed in Duncan et al. (2021) are systematically underestimated for our low-redshift sources due to the small size of the aperture (see §2). Instead of these, we use the M_\star derived from the SED in §3.1. These values are listed in Table 2.

Another method we use to have M_\star estimates is using the method outlined in Zibetti et al. (2009). The underlying principle here is to use optical-NIR color(s) to infer effective stellar mass-to-light ratios (M/L) at each pixel (See Sections 2.4 and 3 of Zibetti et al. 2009). The equation Zibetti et al. (2009) derive for the mass-to-light ratio for the i -band is:

$$\log \left(\frac{M_\star}{L_i} \right) = 1.032 (g - i) - 0.963 \quad (4)$$

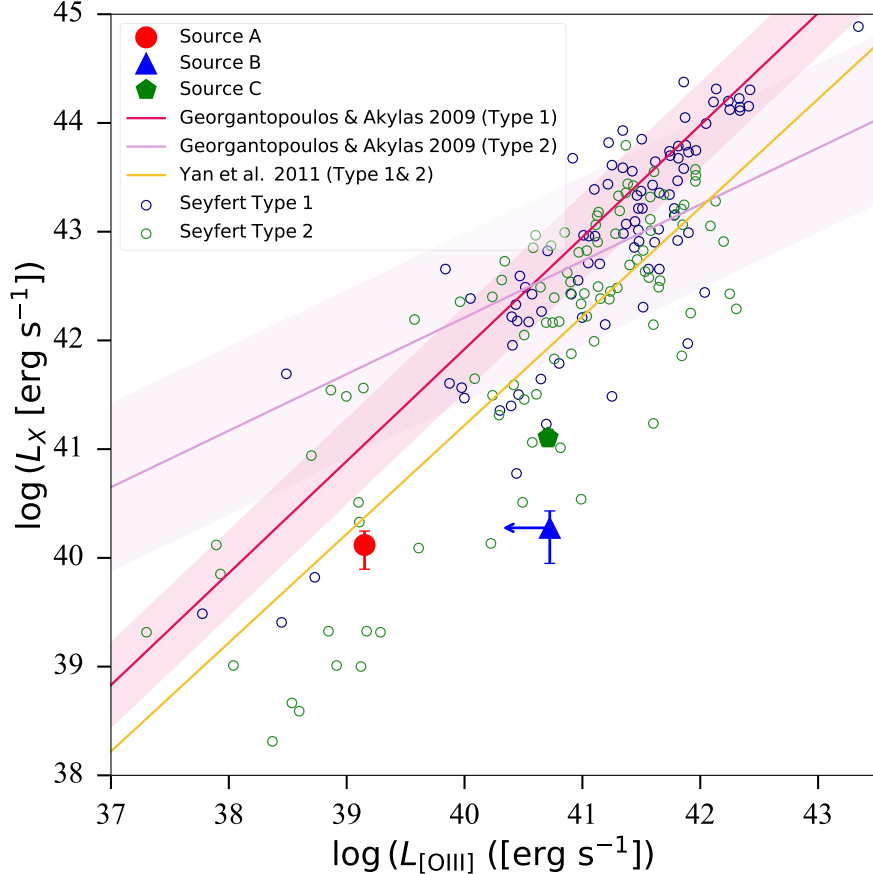


Figure 5. The observed X-ray and [O III] luminosities of the three objects, plotted with various scaling relations from Georgantopoulos & Akylas (2010) and Yan et al. (2011) for Seyfert Type 1 and 2 galaxies. We also plot samples of Seyfert Type 1 (open blue circles) and Type 2 (open green circles) galaxies in the local universe. The [O III] luminosity values plotted here are corrected for extinction. We observe that the three sources lie within the towards the lower luminosity spectrum. The [O III] is considered to be a good proxy for AGN activity since it originates from the narrow-line region, which is outside the obscuring dusty torus (e.g., Bassani et al. 1999; Yan et al. 2011). The [O III] luminosities are consistent with the expected extrapolation of the samples here. Like the L_X - L_{MIR} relation in Figure 4, the deviation from the X-ray suggests obscuration.

We use the SDSS DR17 apparent magnitudes with this relationship (Abdurro'uf et al. 2022). To obtain the luminosity, we adopt a solar absolute i -band magnitude of 4.56 mag (Bell et al. 2003). Errors on M_* are expected to be ~ 0.3 dex and are thought to be dominated by uncertainties in stellar evolution (Conroy et al. 2009).

At wavelengths corresponding to the g and i bands, the SED is dominated by the contribution from the galaxy component and the contribution from the AGN component is negligible. Thus, we can obtain the stellar luminosity of these sources directly from the observed SEDs. The M_* estimates we calculate are listed in Table 3.

Our CIGALE fit does not return uncertainties in M_* . Thus, in Table 2 we report the uncertainties from the mass-to-light ratio estimates and use these as an order of magnitude explanation. The intrinsic uncertainty in the mass-to-light ratio is 0.15 dex (Zibetti et al. 2009).

With the SFR and M_* , we are able to estimate L_{XB} using Equation 2. The values we calculate are summarized in Table 2.

Overall, the analysis in this section suggests that these sources have significant emission from an AGN, and the X-ray emission appears to show significant obscuration. In the next section, we estimate the masses of the central BHs in these systems and analyze if they are IMBHs.

4. BLACK HOLE MASS ESTIMATES

In this section, we estimate the masses of the BHs (M_{BH}) using various scaling relations, to determine whether these galaxies host IMBHs, and to estimate the growth timescales via the observed Eddington ratios. Evidence points towards the scaling of central BH properties with their host galaxies properties like the

Table 2. Properties derived from SED fitting and used to calculate expected emission from X-ray binaries

| Identifier | $\log M_\star$ (M_\odot) | SFR (M_\odot/yr) | $\log L_{\text{H}\alpha}$ (erg s^{-1}) | $\log L_{\text{XB}}$ (erg s^{-1}) | $\log L_{\text{X}}$ (erg s^{-1}) |
|------------|---------------------------------|--------------------------------|--|---|--|
| A | 9.21 | $(1.4 \pm 0.7) \times 10^{-3}$ | $39.10^{+0.06}_{-0.06}$ | 38.2 ± 0.0003 | $40.1^{+0.3}_{-0.1}$ |
| B | 8.83 | 3.2 ± 0.1 | $40.80^{+0.06}_{-0.05}$ | 39.7 ± 0.02 | $40.3^{+0.2}_{-0.1}$ |
| C | 10.43 | $(2.3 \pm 0.1) \times 10^{-2}$ | $40.52^{+0.06}_{-0.05}$ | 39.4 ± 0.0003 | $41.1^{+0.1}_{-0.1}$ |

NOTE—The SED-derived total stellar mass (*Column 2*) and star formation rate (*Column 4*) are used to calculate the galactic-wide emission from X-ray binaries (*Column 6*) following Lehmer et al. (2010). For comparison, we also include the X-ray luminosity calculated from Chandra flux (*Column 7*). The Chandra X-ray luminosity is larger by $\sim 1 - 2$ orders of magnitude. Thus, the X-ray emission detected cannot fully be explained by the presence of X-ray binaries and we attribute it to the presence of AGNs. Since our CIGALE fit does not give errors in the stellar mass, we refer to the mass-to-light ratio intrinsic errors of 0.15 dex as an order of magnitude estimate (Zibetti et al. 2009).

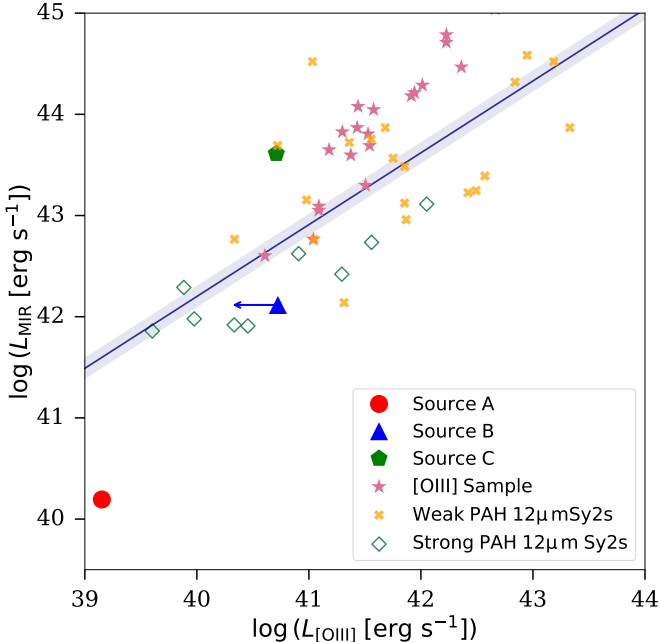


Figure 6. A plot of $L_{[\text{OIII}]}$ vs L_{MIR} , along with the relationship derived by LaMassa et al. (2010). We also plot the samples of [O III] AGN from Adelman-McCarthy et al. (2006) (solid pink stars) and 12 μm samples of weak (solid yellow crosses) and strong (open green diamonds) polycyclic aromatic hydrocarbons (PAHs) Seyfert 2 galaxies from Spinoglio & Malkan (1989). Sources B and C fall within the scatter while A lies near the tail of the linear relationship extrapolated to the low-mass region.

stellar velocity dispersion, mass, IR luminosity etc. The correlations provide an opportunity to study the linked evolution of galaxies and BHs and simultaneously pro-

vide a way to estimate the BH mass via a proxy (Reines & Volonteri 2015). In this paper, we estimate the BH masses using two scaling relations: the $M_{\text{BH}} - \sigma^*$ relation and the $M_{\text{BH}} - M_\star$ relation.

4.1. $M_{\text{BH}} - \sigma^*$

The $M_{\text{BH}} - \sigma^*$ relation is the empirical correlation between the BH mass and the stellar velocity dispersion of the host galaxy. The relation has been studied in several works (e.g., Kormendy & Ho 2013; Saglia et al. 2016; van den Bosch 2016; Krajnović et al. 2018), most notably for high-mass galaxies.

We follow the relation in Greene et al. (2020) which is derived using BH mass samples from Kormendy & Ho (2013), Greene et al. (2016), Krajnović et al. (2018), Nguyen et al. (2018), and Thater et al. (2019). The relation derived is as:

$$\left(\frac{M_{\text{BH}}}{M_\odot} \right) = \alpha + \beta \log \left(\frac{\sigma^*}{160 \text{ km/s}} \right) + \epsilon \quad (5)$$

α , β , and ϵ are determined for different galaxy populations considered in the authors' analysis. We use the values determined for “All, no limits” (all galaxy samples, not including the upper limits on dwarf galaxies)⁴: $\alpha = 7.88 \pm 0.05$, $\beta = 4.34 \pm 0.24$, and $\epsilon = 0.53 \pm 0.04$. The estimates we obtain for the masses are shown in Figure 7 and tabulated in Table 3. Since the errors in

⁴ We use this instead of the “All, with limits” sample (which includes the dwarf galaxies) because the two differ only marginally in their fit parameters. The dwarf galaxies are still plotted in Figure 7 for comparison.

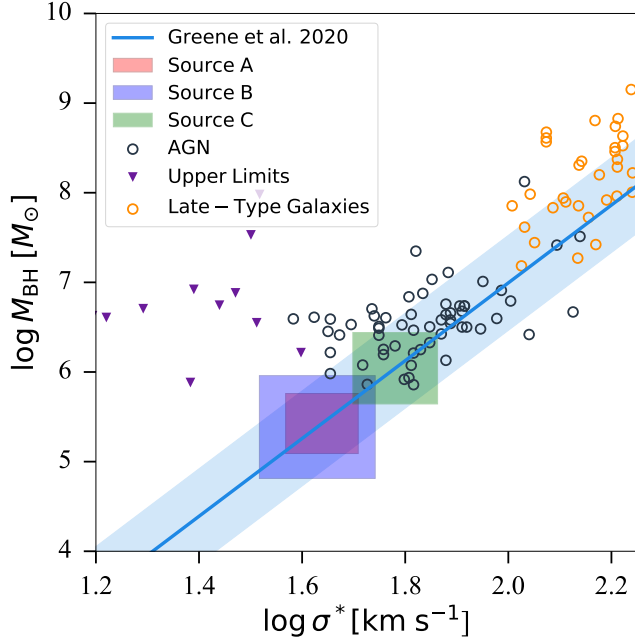


Figure 7. The $M_{\text{BH}} - \sigma^*$ relation following Greene et al. (2020) determined for all galaxy types with no limits. The gray open circles represent the AGN sample from Xiao et al. (2011), open yellow circles are late-type galaxies, and solid purple triangles are the upper limits on dwarf galaxies. The $M_{\text{BH}} - \sigma^*$ relationship shows a scatter at the low mass tail which is in part due to the lack of uniform occupation fraction at lower masses. The values are shown as shaded regions to convey related errors.

M_{BH} arise from the errors in σ^* , the values are shown as shaded rectangles to convey the correlation.

4.2. $M_{\text{BH}} - M_*$

We consider another scaling relation to obtain additional estimates of M_{BH} . The scaling relation between the BH mass and M_* has also been studied in detail (e.g., Kormendy & Ho 2013; Reines & Volonteri 2015; Greene et al. 2020). We use the relations derived in Reines & Volonteri (2015) and Greene et al. (2020) to provide an independent estimate of the BH masses.

Reines & Volonteri (2015) derive the total M_* of a galaxy using photometry following Zibetti et al. (2009). We use the masses calculated in §3.4 for M_* , and estimate M_{BH} using the relationship from Reines & Volonteri (2015):

$$\log\left(\frac{M_{\text{BH}}}{M_{\odot}}\right) = \alpha + \beta \log\left(\frac{M_*}{10^{11}M_{\odot}}\right) \quad (6)$$

where $\alpha = 7.45 \pm 0.08$ and $\beta = 1.05 \pm 0.11$. Greene et al. (2020) presents another equation for the $M_{\text{BH}} - M_*$ scaling relation, derived from an updated sample

of IMBH candidates (as mentioned for the $M_{\text{BH}} - \sigma^*$ relation). We use the “All, no limits” sample:

$$\log\left(\frac{M_{\text{BH}}}{M_{\odot}}\right) = \alpha + \beta \log\left(\frac{M_*}{3 \times 10^{10}M_{\odot}}\right) + \epsilon \quad (7)$$

where $\alpha = 7.56 \pm 0.09$, $\beta = 1.39 \pm 0.13$, and $\epsilon = 0.79 \pm 0.05$. Focusing on the IMBH regime, it is apparent that without upper limits, the fit to late-type galaxies returns a very shallow relation, because the measured M_{BH} values are biased towards higher mass BHs (e.g., Pacucci et al. 2018; Greene et al. 2020).

The scatter in BH and galaxy relationships have been widely studied (e.g., Kormendy & Ho 2013; Saglia et al. 2016; Pacucci et al. 2018). The scatter on the low-mass end is primarily due to the uncertainties in measurements of galaxy properties and due to the presence of only upper limits on some quantities.

4.3. Discussion of scaling relations

The BH mass estimates are listed in Table 3. We report the $M_{\text{BH}} - \sigma^*$ derived BH mass because of the large scatter in the $M_{\text{BH}} - M_*$ relation (especially in the range $M_* \sim 10^9 - 10^{11}M_{\odot}$), and because of the significant deviation between σ and M_* -derived masses for source C. The SDSS image of source C suggests a disk morphology, and its stellar velocity dispersion is well below that expected for a spheroid-dominated system of similar M_* (Leigh et al. 2012), indicating that its stellar morphology is dominated by a disk.

The applicability of the $M_{\text{BH}} - \sigma^*$ relation is debated for low-mass galaxies (e.g., Pacucci et al. 2018; Greene et al. 2020), mainly because σ^* is traditionally defined as the velocity dispersion of stars inside bulges. The slope of the relation changes considerably based on the galaxy population likely due to the bias in M_{BH} measurements toward the most massive BHs. There is also a marked departure in the estimates for mass around $M_{\text{BH}} \leq 10^5 M_{\odot}$ (Pacucci et al. 2018). The observed $M_{\text{BH}} - \sigma^*$ relation favors heavy seed models that make exclusively $M_{\text{BH}} > 10^5 M_{\odot}$. The low-mass tail of the $M_{\text{BH}} - \sigma^*$ relation is now being explored (see Pacucci et al. 2018) since it is believed to provide a stronger, and more fundamental, correlation than $M_{\text{BH}} - M_*$ (e.g., Sesana et al. 2016; Pacucci et al. 2018).

SDSS recommends users not rely upon data with $\sigma^* < 70 \text{ km s}^{-1}$ due to the typical signal-to-noise ratio and the instrumental resolution of the spectra (for more information see Almeida et al. 2023). Since our sources are low-mass and hence have small σ^* , their velocity

Table 3. A tabulation of the BH mass estimates and Eddington ratios calculated using various scaling relationships

| Identifier | σ^* (km s $^{-1}$) | $M_{\text{BH}} - \sigma^*$ $\log M_{\text{BH}}$ | $M_{\text{BH}} - M_*(1)$ $\log M_{\text{BH}}$ | $M_{\text{BH}} - M_*(2)$ $\log M_{\text{BH}}$ | log Eddington limit (erg s $^{-1}$) | Eddington ratio |
|------------|-------------------------------|--|--|--|---|-----------------|
| A | 43.5 ± 7.6 | 5.42 ± 0.33 | 5.58 | 5.80 | 43.52 | 0.02 |
| B | 42.6 ± 10.2 | 5.38 ± 0.57 | 5.17 | 5.27 | 43.48 | 0.39 |
| C | 60.3 ± 12.5 | 6.04 ± 0.40 | 6.85 | 7.49 | 44.13 | 0.13 |

NOTE—The BH masses (in M_\odot) are calculated using different scaling relations involving the host galaxy's velocity dispersion, σ^* , and total stellar mass, M_* . *Column 4* uses the relation in Reines & Volonteri (2015) and *Column 5* uses Greene et al. (2020). The M_{BH} estimates from the $M_{\text{BH}} - M_*$ relation do not have uncertainties listed because the M_* estimates from the CIGALE SED fitting do not have errors. It is also important to note that the uncertainties in the relation dominate over the stellar mass uncertainties.

dispersions fall below the recommended limit. To check the validity of our estimate, we carried out an analysis of the SDSS spectra from which the velocity dispersions were derived. We confirmed that the σ^* measurements reliable in terms of the strength of the relevant absorption lines, the spectral resolution of the data, and the model fit to the flux to determine the velocity dispersion. We first fit Gaussians to the calcium absorption and neon emission lines to check the σ^* derived from the fit width against that reported by SDSS. For a more rigorous analysis, we use the `ppxf` Python package (Cappellari 2022) to carry out a detailed analysis using both photometric and spectroscopic data. Using stellar and gas templates, we fit a two-component model (V: velocity and σ^* : velocity dispersion) to the data. We find that the estimates are in good agreement with the SDSS values and fall within the reported SDSS errors.

With these considerations in mind, we adopt the σ^* -derived BH mass in calculating the Eddington ratio for all three sources. The masses of the three sources are $\sim 10^5 - 10^6 M_\odot$, as listed in Table 3. To compute the Eddington ratio, we calculate the computed the $15 \mu\text{m}$ bolometric luminosity from our SED fitting and estimate the bolometric luminosity, using bolometric correction from Shen et al. (2020). We report the Eddington limit and the ratio in Table 3. We see that the Eddington ratios are of the order of $10^{-2} - 10^{-1}$ meaning that the BHs are accreting at relatively high rates typical of local Seyfert galaxies. Their Eddington ratios are consistent with thin-disk accretion (Shakura & Sunyaev 1973) and thus they lie in the radiatively efficient regime of AGNs.

5. CONCLUSION

We analyze the nature of three dwarf galaxies with strong X-ray emission in the Boötes field and investigate

whether they obtain accreting nuclear BHs. These targets are selected by cross-matching two catalogs: Masini et al. (2020) (X-ray detections) and Duncan et al. (2021) (estimates of total stellar mass). From the cross-match we make cuts to select low-mass galaxies in the local universe. We rely on X-ray detections to identify AGN because they are one of the clearest indicators of AGN activity in a galaxy (e.g., Miller et al. 2015; Baldassare et al. 2015; Pardo et al. 2016). We analyze the source of their emission lines using a narrow-line BPT diagnostic diagram. We find that two of the sources fall in the AGN region while one is in the SF region, but consistent with the AGN region within the uncertainties. We use observations in the UV, optical, and IR to compute the SEDs for our galaxies and fit them using CIGALE using various combinations of stellar and AGN templates. With the MIR and [O III] luminosities, we are able to assess them as likely AGN candidates. To confirm that the X-ray emissions we observe originate from AGNs and not galactic-wide X-ray binaries, we calculate the $L_{\text{H}\alpha}$ luminosity and SFR for each of our galaxies.

By analyzing the deviation from the linear luminosity relationships, we conclude that these sources are considerably obscured in the X-rays. We report upper limits on the column densities using the BORUS model in Carroll et al. (2021). Through our analysis, we find that the sources show clear signs of hosting AGNs. We use scaling relations like the $M_{\text{BH}} - \sigma^*$ and $M_{\text{BH}} - M_*$ to estimate the masses of the BHs. The morphology of source C in Figure 1 and the $M_* - \sigma^*$ trends for spheroids, we believe that it is a disc galaxy. Thus, we choose to use the σ^* -derived relation for the BH masses for all three sources to be consistent. Their masses fall in the range of $10^5 - 10^6 M_\odot$.

By comparing these estimates to the IMBHs studied in literature (e.g., Reines & Volonteri 2015; Greene et al.

2020), we conclude that our sources are good candidates for the same. We estimate the Eddington ratios of the BHs using the $M_{\text{BH}} - \sigma^*$ -determined value for their masses, which are of the orders of 10^{-2} – 10^{-1} . These ratios suggest that BHs are accreting at rates characteristic of optically-thick, radiatively efficient accretion flows.

To place these dwarf galaxies in the broader context, it is helpful to consider the fraction of the dwarf galaxy population that we recover as AGNs. From Duncan et al. (2021)’s compilation, there are 66 galaxies in the Boötes field with $M_* < 10^{9.5} M_\odot$ and spectroscopic redshift $z < 0.05$. As all of our targets have spectroscopic redshifts, comparing them to other dwarf galaxies that have similar observations would be a more accurate estimate of population fractions. Using the method described in §3.4 we note that stellar mass estimates of these sources are comparable to our three targets. Most sources that have spectroscopic redshifts also have listed velocity dispersions. Using these numbers, we can conclude that roughly 5% of all local dwarf galaxies host AGNs. This is an important statistic in uncovering the presence of AGNs in dwarf galaxies.

Future research in this field could include a deeper analysis of current IMBH candidates. In this study, we identified our targets using X-ray data that was part of a larger observation cycle. More focused spectra and large fields of X-ray, optical, and infrared of local dwarf galaxies could help us to better identify IMBHs. Dynamical mass estimates would also allow us to place constraints on BH-galaxy scaling relations for dwarfs. Additionally, a majority of the AGN activity in the universe is obscured (e.g., Ueda et al. 2014; Hickox & Alexander 2018; Ananna et al. 2019), meaning that studying obscured AGNs in dwarf galaxies can provide a more complete picture of the population fraction and properties of these low-mass BHs.

ACKNOWLEDGEMENTS

R.A.P. acknowledges support from the James O. Freedman Presidential Scholarship. G.C.P. acknowledges support from the Dartmouth Fellowship. R.A.P. would like to thank Jenny Greene, Kelly Whalen, and Stephanie Podjed for their guidance and helpful discussions.

Funding for the Sloan Digital Sky Survey IV has been provided by the Alfred P. Sloan Foundation, the U.S. Department of Energy Office of Science, and the Participating Institutions. SDSS-IV acknowledges support and resources from the Center for High-Performance Computing at the University of Utah. The SDSS website is www.sdss4.org. SDSS-IV is managed by the Astrophys-

ical Research Consortium for the Participating Institutions of the SDSS Collaboration including the Brazilian Participation Group, the Carnegie Institution for Science, Carnegie Mellon University, Center for Astrophysics — Harvard & Smithsonian, the Chilean Participation Group, the French Participation Group, Instituto de Astrofísica de Canarias, The Johns Hopkins University, Kavli Institute for the Physics and Mathematics of the Universe (IPMU) / University of Tokyo, the Korean Participation Group, Lawrence Berkeley National Laboratory, Leibniz Institut für Astrophysik Potsdam (AIP), Max-Planck-Institut für Astronomie (MPIA Heidelberg), Max-Planck-Institut für Astrophysik (MPA Garching), Max-Planck-Institut für Extraterrestrische Physik (MPE), National Astronomical Observatories of China, New Mexico State University, New York University, University of Notre Dame, Observatório Nacional / MCTI, The Ohio State University, Pennsylvania State University, Shanghai Astronomical Observatory, United Kingdom Participation Group, Universidad Nacional Autónoma de México, University of Arizona, University of Colorado Boulder, University of Oxford, University of Portsmouth, University of Utah, University of Virginia, University of Washington, University of Wisconsin, Vanderbilt University, and Yale University.

This publication makes use of data products from the Wide-field Infrared Survey Explorer, which is a joint project of the University of California, Los Angeles, and the Jet Propulsion Laboratory/California Institute of Technology, funded by the National Aeronautics and Space Administration.

This research has made use of the NASA/IPAC Extragalactic Database (NED), which is funded by the National Aeronautics and Space Administration and operated by the California Institute of Technology.

HIFI has been designed and built by a consortium of institutes and university departments from across Europe, Canada and the United States under the leadership of SRON Netherlands Institute for Space Research, Groningen, The Netherlands and with major contributions from Germany, France and the US. Consortium members are: Canada: CSA, U.Waterloo; France: CESR, LAB, LERMA, IRAM; Germany: KOSMA, MPIfR, MPS; Ireland, NUI Maynooth; Italy: ASI, IFSI-INAF, Osservatorio Astrofisico di Arcetri-INAF; Netherlands: SRON, TUD; Poland: CAMK, CBK; Spain: Observatorio Astronómico Nacional (IGN), Centro de Astrobiología (CSIC-INTA). Sweden: Chalmers University of Technology - MC2, RSS & GARD; Onsala Space Observatory; Swedish National Space Board, Stockholm University - Stockholm Observatory;

Switzerland: ETH Zurich, FHNW; USA: Caltech, JPL, NHSC.

PACS has been developed by a consortium of institutes led by MPE (Germany) and including UVIE (Austria); KU Leuven, CSL, IMEC (Belgium); CEA, LAM (France); MPIA (Germany); INAF-IFSI/OAA/OAP/OAT, LENS, SISSA (Italy); IAC (Spain). This development has been supported by the funding agencies BMVIT (Austria), ESA-PRODEX (Belgium), CEA/CNES (France), DLR (Germany), ASI/INAF (Italy), and CICYT/MCYT (Spain).

SPIRE has been developed by a consortium of institutes led by Cardiff University (UK) and including Univ. Lethbridge (Canada); NAOC (China); CEA, LAM (France); IFSI, Univ. Padua (Italy); IAC (Spain); Stockholm Observatory (Sweden); Impe-

rial College London, RAL, UCL-MSSL, UKATC, Univ. Sussex (UK); and Caltech, JPL, NHSC, Univ. Colorado (USA). This development has been supported by national funding agencies: CSA (Canada); NAOC (China); CEA, CNES, CNRS (France); ASI (Italy); MCINN (Spain); SNSB (Sweden); STFC, UKSA (UK); and NASA (USA).

Most of this work has been carried out at Dartmouth College which stands on the lands of the Abenaki and other Algonquin peoples.

Facilities: CXO, DESI, NED, GALEX, Sloan

Software: astropy (Astropy Collaboration et al. 2018), TOPCAT (Shopbell et al. 2005), CIGALE (Burgarella et al. 2005; Boquien et al. 2019), ppxf (Vazdekis et al. 2016; Cappellari 2022)

REFERENCES

- Abdurro'uf, Accetta, K., Aerts, C., et al. 2022, ApJS, 259, 35, doi: [10.3847/1538-4365/ac4414](https://doi.org/10.3847/1538-4365/ac4414)
- Adelman-McCarthy, J. K., Agüeros, M. A., Allam, S. S., et al. 2006, ApJS, 162, 38, doi: [10.1086/497917](https://doi.org/10.1086/497917)
- Almeida, A., Anderson, S. F., Argudo-Fernández, M., et al. 2023, ApJS, 267, 44, doi: [10.3847/1538-4365/acda98](https://doi.org/10.3847/1538-4365/acda98)
- Ananna, T. T., Treister, E., Urry, C. M., et al. 2019, ApJ, 871, 240, doi: [10.3847/1538-4357/aafb77](https://doi.org/10.3847/1538-4357/aafb77)
- Assef, R. J., Kochanek, C. S., Brodwin, M., et al. 2010, ApJ, 713, 970, doi: [10.1088/0004-637X/713/2/970](https://doi.org/10.1088/0004-637X/713/2/970)
- Astropy Collaboration, Price-Whelan, A. M., Sipőcz, B. M., et al. 2018, AJ, 156, 123, doi: [10.3847/1538-3881/aabc4f](https://doi.org/10.3847/1538-3881/aabc4f)
- Baldassare, V. F., Dickey, C., Geha, M., & Reines, A. E. 2020, ApJL, 898, L3, doi: [10.3847/2041-8213/aba0c1](https://doi.org/10.3847/2041-8213/aba0c1)
- Baldassare, V. F., Reines, A. E., Gallo, E., & Greene, J. E. 2015, ApJL, 809, L14, doi: [10.1088/2041-8205/809/1/L14](https://doi.org/10.1088/2041-8205/809/1/L14)
- Baldwin, J. A., Phillips, M. M., & Terlevich, R. 1981, PASP, 93, 5, doi: [10.1086/130766](https://doi.org/10.1086/130766)
- Bambi, C. 2020, in Multifrequency Behaviour of High Energy Cosmic Sources - XIII. 3-8 June 2019. Palermo, 28, doi: [10.22323/1.362.0028](https://doi.org/10.22323/1.362.0028)
- Barro, G., Perez-Gonzalez, P. G., Kocevski, D. D., et al. 2023, arXiv e-prints, arXiv:2305.14418, doi: [10.48550/arXiv.2305.14418](https://doi.org/10.48550/arXiv.2305.14418)
- Barth, A., Ho, L., & Sargent, W. 2004, in Astronomical Society of the Pacific Conference Series, Vol. 311, AGN Physics with the Sloan Digital Sky Survey, ed. G. T. Richards & P. B. Hall, 91, doi: [10.48550/arXiv.astro-ph/0310435](https://doi.org/10.48550/arXiv.astro-ph/0310435)
- Bassani, L., Dadina, M., Maiolino, R., et al. 1999, ApJS, 121, 473, doi: [10.1086/313202](https://doi.org/10.1086/313202)
- Begelman, M. C., Volonteri, M., & Rees, M. J. 2006, MNRAS, 370, 289, doi: [10.1111/j.1365-2966.2006.10467.x](https://doi.org/10.1111/j.1365-2966.2006.10467.x)
- Bell, E. F., McIntosh, D. H., Katz, N., & Weinberg, M. D. 2003, ApJS, 149, 289, doi: [10.1086/378847](https://doi.org/10.1086/378847)
- Blanton, M. R., Bershadsky, M. A., Abolfathi, B., et al. 2017, AJ, 154, 28, doi: [10.3847/1538-3881/aa7567](https://doi.org/10.3847/1538-3881/aa7567)
- Bongiorno, A., Mignoli, M., Zamorani, G., et al. 2010, A&A, 510, A56, doi: [10.1051/0004-6361/200913229](https://doi.org/10.1051/0004-6361/200913229)
- Boquien, M., Burgarella, D., Roehlly, Y., et al. 2019, A&A, 622, A103, doi: [10.1051/0004-6361/201834156](https://doi.org/10.1051/0004-6361/201834156)
- Brandt, W. N., & Alexander, D. M. 2015, A&A Rev, 23, 1, doi: [10.1007/s00159-014-0081-z](https://doi.org/10.1007/s00159-014-0081-z)
- Burgarella, D., Buat, V., & Iglesias-Páramo, J. 2005, MNRAS, 360, 1413, doi: [10.1111/j.1365-2966.2005.09131.x](https://doi.org/10.1111/j.1365-2966.2005.09131.x)
- Calzetti, D. 2013, in Secular Evolution of Galaxies, ed. J. Falcón-Barroso & J. H. Knapen, 419, doi: [10.48550/arXiv.1208.2997](https://doi.org/10.48550/arXiv.1208.2997)
- Calzetti, D., Armus, L., Bohlin, R. C., et al. 2000, ApJ, 533, 682, doi: [10.1086/308692](https://doi.org/10.1086/308692)
- Cappellari, M. 2022, arXiv e-prints, arXiv:2208.14974, doi: [10.48550/arXiv.2208.14974](https://doi.org/10.48550/arXiv.2208.14974)
- Carroll, C. M., Ananna, T. T., Hickox, R. C., et al. 2023, arXiv e-prints, arXiv:2303.08813, doi: [10.48550/arXiv.2303.08813](https://doi.org/10.48550/arXiv.2303.08813)
- Carroll, C. M., Hickox, R. C., Masini, A., et al. 2021, ApJ, 908, 185, doi: [10.3847/1538-4357/abd185](https://doi.org/10.3847/1538-4357/abd185)
- Celotti, A., Miller, J. C., & Sciama, D. W. 1999, Classical and Quantum Gravity, 16, A3, doi: [10.1088/0264-9381/16/12A/301](https://doi.org/10.1088/0264-9381/16/12A/301)
- Chen, C.-T. J., Hickox, R. C., Goulding, A. D., et al. 2017, ApJ, 837, 145, doi: [10.3847/1538-4357/837/2/145](https://doi.org/10.3847/1538-4357/837/2/145)

- Conroy, C., Gunn, J. E., & White, M. 2009, ApJ, 699, 486, doi: [10.1088/0004-637X/699/1/486](https://doi.org/10.1088/0004-637X/699/1/486)
- Dale, D. A., Helou, G., Magdis, G. E., et al. 2014, ApJ, 784, 83, doi: [10.1088/0004-637X/784/1/83](https://doi.org/10.1088/0004-637X/784/1/83)
- Duncan, K. J., Kondapally, R., Brown, M. J. I., et al. 2021, A&A, 648, A4, doi: [10.1051/0004-6361/202038809](https://doi.org/10.1051/0004-6361/202038809)
- Feltre, A., Charlot, S., & Gutkin, J. 2016, MNRAS, 456, 3354, doi: [10.1093/mnras/stv2794](https://doi.org/10.1093/mnras/stv2794)
- Ferrara, A., Salvadori, S., Yue, B., & Schleicher, D. 2014, MNRAS, 443, 2410, doi: [10.1093/mnras/stu1280](https://doi.org/10.1093/mnras/stu1280)
- Filippenko, A. V., & Ho, L. C. 2003, ApJL, 588, L13, doi: [10.1086/375361](https://doi.org/10.1086/375361)
- Filippenko, A. V., & Sargent, W. L. W. 1989, ApJL, 342, L11, doi: [10.1086/185472](https://doi.org/10.1086/185472)
- Gandhi, P., Horst, H., Smette, A., et al. 2009, A&A, 502, 457, doi: [10.1051/0004-6361/200811368](https://doi.org/10.1051/0004-6361/200811368)
- Georgantopoulos, I., & Akylas, A. 2010, A&A, 509, A38, doi: [10.1051/0004-6361/200912943](https://doi.org/10.1051/0004-6361/200912943)
- Gilfanov, M. 2004, MNRAS, 349, 146, doi: [10.1111/j.1365-2966.2004.07473.x](https://doi.org/10.1111/j.1365-2966.2004.07473.x)
- Greene, J. E., Strader, J., & Ho, L. C. 2020, ARA&A, 58, 257, doi: [10.1146/annurev-astro-032620-021835](https://doi.org/10.1146/annurev-astro-032620-021835)
- Greene, J. E., Seth, A., Kim, M., et al. 2016, ApJL, 826, L32, doi: [10.3847/2041-8205/826/2/L32](https://doi.org/10.3847/2041-8205/826/2/L32)
- Greene, J. E., Labbe, I., Goulding, A. D., et al. 2023, arXiv e-prints, arXiv:2309.05714, doi: [10.48550/arXiv.2309.05714](https://doi.org/10.48550/arXiv.2309.05714)
- Grimm, H. J., Gilfanov, M., & Sunyaev, R. 2003, MNRAS, 339, 793, doi: [10.1046/j.1365-8711.2003.06224.x](https://doi.org/10.1046/j.1365-8711.2003.06224.x)
- Heckman, T. M., Kauffmann, G., Brinchmann, J., et al. 2004, ApJ, 613, 109, doi: [10.1086/422872](https://doi.org/10.1086/422872)
- Heckman, T. M., Ptak, A., Hornschemeier, A., & Kauffmann, G. 2005, ApJ, 634, 161, doi: [10.1086/491665](https://doi.org/10.1086/491665)
- Heger, A., Fryer, C. L., Woosley, S. E., Langer, N., & Hartmann, D. H. 2003, ApJ, 591, 288, doi: [10.1086/375341](https://doi.org/10.1086/375341)
- Hickox, R. C., & Alexander, D. M. 2018, ARA&A, 56, 625, doi: [10.1146/annurev-astro-081817-051803](https://doi.org/10.1146/annurev-astro-081817-051803)
- Jannuzzi, B. T., Dey, A., & NDWFS Team. 1999, in American Astronomical Society Meeting Abstracts, Vol. 195, American Astronomical Society Meeting Abstracts, 12.07
- Jardel, J. R., & Gebhardt, K. 2012, ApJ, 746, 89, doi: [10.1088/0004-637X/746/1/89](https://doi.org/10.1088/0004-637X/746/1/89)
- Jiang, Y.-F., Stone, J. M., & Davis, S. W. 2019, ApJ, 880, 67, doi: [10.3847/1538-4357/ab29ff](https://doi.org/10.3847/1538-4357/ab29ff)
- Johnson, J. L., Whalen, D. J., Li, H., & Holz, D. E. 2013, ApJ, 771, 116, doi: [10.1088/0004-637X/771/2/116](https://doi.org/10.1088/0004-637X/771/2/116)
- Jones, M. L., Hickox, R. C., Black, C. S., et al. 2016, ApJ, 826, 12, doi: [10.3847/0004-637X/826/1/12](https://doi.org/10.3847/0004-637X/826/1/12)
- Kewley, L. J., Groves, B., Kauffmann, G., & Heckman, T. 2006, MNRAS, 372, 961, doi: [10.1111/j.1365-2966.2006.10859.x](https://doi.org/10.1111/j.1365-2966.2006.10859.x)
- Kochanek, C. S., Eisenstein, D. J., Cool, R. J., et al. 2012, ApJS, 200, 8, doi: [10.1088/0067-0049/200/1/8](https://doi.org/10.1088/0067-0049/200/1/8)
- Kokorev, V., Fujimoto, S., Labbe, I., et al. 2023, arXiv e-prints, arXiv:2308.11610, doi: [10.48550/arXiv.2308.11610](https://doi.org/10.48550/arXiv.2308.11610)
- Kormendy, J., & Ho, L. C. 2013, ARA&A, 51, 511, doi: [10.1146/annurev-astro-082708-101811](https://doi.org/10.1146/annurev-astro-082708-101811)
- Krajnović, D., Cappellari, M., McDermid, R. M., et al. 2018, MNRAS, 477, 3030, doi: [10.1093/mnras/sty778](https://doi.org/10.1093/mnras/sty778)
- Kunth, D., Sargent, W. L. W., & Bothun, G. D. 1987, AJ, 93, 29, doi: [10.1086/114287](https://doi.org/10.1086/114287)
- LaMassa, S. M., Heckman, T. M., Ptak, A., et al. 2010, ApJ, 720, 786, doi: [10.1088/0004-637X/720/1/786](https://doi.org/10.1088/0004-637X/720/1/786)
- Larson, R. L., Finkelstein, S. L., Kocevski, D. D., et al. 2023, arXiv e-prints, arXiv:2303.08918, doi: [10.48550/arXiv.2303.08918](https://doi.org/10.48550/arXiv.2303.08918)
- Latimer, L. J., Reines, A. E., Hainline, K. N., Greene, J. E., & Stern, D. 2021, ApJ, 914, 133, doi: [10.3847/1538-4357/abfe0c](https://doi.org/10.3847/1538-4357/abfe0c)
- Lehmer, B. D., Alexander, D. M., Bauer, F. E., et al. 2010, ApJ, 724, 559, doi: [10.1088/0004-637X/724/1/559](https://doi.org/10.1088/0004-637X/724/1/559)
- Leigh, N., Böker, T., & Knigge, C. 2012, MNRAS, 424, 2130, doi: [10.1111/j.1365-2966.2012.21365.x](https://doi.org/10.1111/j.1365-2966.2012.21365.x)
- Loeb, A., & Rasio, F. A. 1994, ApJ, 432, 52, doi: [10.1086/174548](https://doi.org/10.1086/174548)
- Lynden-Bell, D. 1969, Nature, 223, 690, doi: [10.1038/223690a0](https://doi.org/10.1038/223690a0)
- Madau, P., & Rees, M. J. 2001, ApJL, 551, L27, doi: [10.1086/319848](https://doi.org/10.1086/319848)
- Magorrian, J., Tremaine, S., Richstone, D., et al. 1998, AJ, 115, 2285, doi: [10.1086/300353](https://doi.org/10.1086/300353)
- Magris C., G., Mateu P., J., Mateu, C., et al. 2015, PASP, 127, 16, doi: [10.1086/679742](https://doi.org/10.1086/679742)
- Mancini, L., & Feoli, A. 2012, A&A, 537, A48, doi: [10.1051/0004-6361/201117168](https://doi.org/10.1051/0004-6361/201117168)
- Marconi, A., & Hunt, L. K. 2003, ApJL, 589, L21, doi: [10.1086/375804](https://doi.org/10.1086/375804)
- Martin, D. C., Fanson, J., Schiminovich, D., et al. 2005, ApJL, 619, L1, doi: [10.1086/426387](https://doi.org/10.1086/426387)
- Marziani, P., D’Onofrio, M., Bettoni, D., et al. 2017, A&A, 599, A83, doi: [10.1051/0004-6361/201628941](https://doi.org/10.1051/0004-6361/201628941)
- Masini, A., Hickox, R. C., Carroll, C. M., et al. 2020, ApJS, 251, 2, doi: [10.3847/1538-4365/abb607](https://doi.org/10.3847/1538-4365/abb607)
- Miller, B. P., Gallo, E., Greene, J. E., et al. 2015, ApJ, 799, 98, doi: [10.1088/0004-637X/799/1/98](https://doi.org/10.1088/0004-637X/799/1/98)
- Miller, M. C., & Hamilton, D. P. 2002, MNRAS, 330, 232, doi: [10.1046/j.1365-8711.2002.05112.x](https://doi.org/10.1046/j.1365-8711.2002.05112.x)

- Mulchaey, J. S., Koratkar, A., Ward, M. J., et al. 1994, ApJ, 436, 586, doi: [10.1086/174933](https://doi.org/10.1086/174933)
- Nandra, K. 2006, MNRAS, 368, L62, doi: [10.1111/j.1745-3933.2006.00158.x](https://doi.org/10.1111/j.1745-3933.2006.00158.x)
- Neumayer, N., & Walcher, C. J. 2012, Advances in Astronomy, 2012, 709038, doi: [10.1155/2012/709038](https://doi.org/10.1155/2012/709038)
- Nguyen, D. D., Seth, A. C., Neumayer, N., et al. 2018, ApJ, 858, 118, doi: [10.3847/1538-4357/aabe28](https://doi.org/10.3847/1538-4357/aabe28)
- Pacucci, F., Loeb, A., Mezcua, M., & Martín-Navarro, I. 2018, ApJL, 864, L6, doi: [10.3847/2041-8213/aad8b2](https://doi.org/10.3847/2041-8213/aad8b2)
- Padovani, P., Alexander, D. M., Assef, R. J., et al. 2017, A&A Rv, 25, 2, doi: [10.1007/s00159-017-0102-9](https://doi.org/10.1007/s00159-017-0102-9)
- Pardo, K., Goulding, A. D., Greene, J. E., et al. 2016, ApJ, 831, 203, doi: [10.3847/0004-637X/831/2/203](https://doi.org/10.3847/0004-637X/831/2/203)
- Park, T., Kashyap, V. L., Siemiginowska, A., et al. 2006, ApJ, 652, 610, doi: [10.1086/507406](https://doi.org/10.1086/507406)
- Planck Collaboration, Ade, P. A. R., Aghanim, N., et al. 2016, A&A, 594, A13, doi: [10.1051/0004-6361/201525830](https://doi.org/10.1051/0004-6361/201525830)
- Portegies Zwart, S. F., & McMillan, S. L. W. 2002, ApJ, 576, 899, doi: [10.1086/341798](https://doi.org/10.1086/341798)
- Rees, M. J. 1984, ARA&A, 22, 471, doi: [10.1146/annurev.aa.22.090184.002351](https://doi.org/10.1146/annurev.aa.22.090184.002351)
- Reines, A. E., Greene, J. E., & Geha, M. 2013, ApJ, 775, 116, doi: [10.1088/0004-637X/775/2/116](https://doi.org/10.1088/0004-637X/775/2/116)
- Reines, A. E., & Volonteri, M. 2015, ApJ, 813, 82, doi: [10.1088/0004-637X/813/2/82](https://doi.org/10.1088/0004-637X/813/2/82)
- Remillard, R. A., & McClintock, J. E. 2006, ARA&A, 44, 49, doi: [10.1146/annurev.astro.44.051905.092532](https://doi.org/10.1146/annurev.astro.44.051905.092532)
- Saglia, R. P., Opitsch, M., Erwin, P., et al. 2016, ApJ, 818, 47, doi: [10.3847/0004-637X/818/1/47](https://doi.org/10.3847/0004-637X/818/1/47)
- Salpeter, E. E. 1964, ApJ, 140, 796, doi: [10.1086/147973](https://doi.org/10.1086/147973)
- Sesana, A., Shankar, F., Bernardi, M., & Sheth, R. K. 2016, MNRAS, 463, L6, doi: [10.1093/mnrasl/slw139](https://doi.org/10.1093/mnrasl/slw139)
- Shakura, N. I., & Sunyaev, R. A. 1973, A&A, 24, 337
- Shen, X., Hopkins, P. F., Faucher-Giguère, C.-A., et al. 2020, MNRAS, 495, 3252, doi: [10.1093/mnras/staa1381](https://doi.org/10.1093/mnras/staa1381)
- Shirley, R., Duncan, K., Campos Varillas, M. C., et al. 2021, MNRAS, 507, 129, doi: [10.1093/mnras/stab1526](https://doi.org/10.1093/mnras/stab1526)
- Shopbell, P., Britton, M., & Ebert, R. 2005, Astronomical Data Analysis Software and Systems XIV, 347
- Spinoglio, L., & Malkan, M. A. 1989, ApJ, 342, 83, doi: [10.1086/167577](https://doi.org/10.1086/167577)
- Stern, D. 2015, ApJ, 807, 129, doi: [10.1088/0004-637X/807/2/129](https://doi.org/10.1088/0004-637X/807/2/129)
- Taylor, P., & Kobayashi, C. 2014, MNRAS, 442, 2751, doi: [10.1093/mnras/stu983](https://doi.org/10.1093/mnras/stu983)
- Thater, S., Krajanović, D., Cappellari, M., et al. 2019, A&A, 625, A62, doi: [10.1051/0004-6361/201834808](https://doi.org/10.1051/0004-6361/201834808)
- Ueda, Y., Akiyama, M., Hasinger, G., Miyaji, T., & Watson, M. G. 2014, ApJ, 786, 104, doi: [10.1088/0004-637X/786/2/104](https://doi.org/10.1088/0004-637X/786/2/104)
- van den Bosch, R. C. E. 2016, ApJ, 831, 134, doi: [10.3847/0004-637X/831/2/134](https://doi.org/10.3847/0004-637X/831/2/134)
- Vazdekis, A., Koleva, M., Ricciardelli, E., Röck, B., & Falcón-Barroso, J. 2016, MNRAS, 463, 3409, doi: [10.1093/mnras/stw2231](https://doi.org/10.1093/mnras/stw2231)
- Vito, F., Brandt, W. N., Yang, G., et al. 2018, MNRAS, 473, 2378, doi: [10.1093/mnras/stx2486](https://doi.org/10.1093/mnras/stx2486)
- Volonteri, M., Habouzit, M., & Colpi, M. 2021, Nature Reviews Physics, 3, 732, doi: [10.1038/s42254-021-00364-9](https://doi.org/10.1038/s42254-021-00364-9)
- Volonteri, M., & Reines, A. E. 2016, ApJL, 820, L6, doi: [10.3847/2041-8205/820/1/L6](https://doi.org/10.3847/2041-8205/820/1/L6)
- Wasleske, E. J., Baldassare, V. F., & Carroll, C. M. 2022, ApJ, 933, 37, doi: [10.3847/1538-4357/ac715b](https://doi.org/10.3847/1538-4357/ac715b)
- Werner, M. W., Roellig, T. L., Low, F. J., et al. 2004, ApJS, 154, 1, doi: [10.1086/422992](https://doi.org/10.1086/422992)
- Whalen, D. J., & Fryer, C. L. 2012, ApJL, 756, L19, doi: [10.1088/2041-8205/756/1/L19](https://doi.org/10.1088/2041-8205/756/1/L19)
- Woosley, S. E. 2017, ApJ, 836, 244, doi: [10.3847/1538-4357/836/2/244](https://doi.org/10.3847/1538-4357/836/2/244)
- Wright, E. L., Eisenhardt, P. R. M., Mainzer, A. K., et al. 2010, AJ, 140, 1868, doi: [10.1088/0004-6256/140/6/1868](https://doi.org/10.1088/0004-6256/140/6/1868)
- Xiao, T., Barth, A. J., Greene, J. E., et al. 2011, ApJ, 739, 28, doi: [10.1088/0004-637X/739/1/28](https://doi.org/10.1088/0004-637X/739/1/28)
- Yamada, S., Ueda, Y., Herrera-Endoqui, M., et al. 2023, ApJS, 265, 37, doi: [10.3847/1538-4365/acb349](https://doi.org/10.3847/1538-4365/acb349)
- Yan, R., Ho, L. C., Newman, J. A., et al. 2011, ApJ, 728, 38, doi: [10.1088/0004-637X/728/1/38](https://doi.org/10.1088/0004-637X/728/1/38)
- Zibetti, S., Charlot, S., & Rix, H.-W. 2009, MNRAS, 400, 1181, doi: [10.1111/j.1365-2966.2009.15528.x](https://doi.org/10.1111/j.1365-2966.2009.15528.x)